

# Learning from humans: combining imitation and deep reinforcement learning to accomplish human-level performance on a virtual foraging task

Vittorio Giammarino <sup>1\*</sup>, Matthew F Dunne <sup>4,5,6</sup>, Kylie N Moore <sup>4,5,6</sup>, Michael E Hasselmo <sup>6</sup>, Chantal E Stern <sup>4,6</sup>, Ioannis Ch. Paschalidis <sup>1,2,3</sup>

**1** Division of Systems Engineering, Boston University, Boston, MA 02446, USA.

**2** Dept. of Electrical and Computer Engineering, Boston University, Boston, MA 02446, USA.

**3** Dept. of Biomedical Engineering, Boston University, Boston, MA 02215, USA.

**4** Cognitive Neuroimaging Center, Boston University, Boston, MA 02215, USA.

**5** Graduate Program for Neuroscience, Boston University, Boston, MA 02215, USA.

**6** Center for Systems Neuroscience, Boston University, Boston, MA 02215, USA.

¶Membership list can be found in the Acknowledgments section.

\* vittoriogiammarino@gmail.com

## Abstract

We develop a method to learn bio-inspired foraging policies using human data. We conduct an experiment where humans are virtually immersed in an open field foraging environment and are trained to collect the highest amount of rewards. A Markov Decision Process (MDP) framework is introduced to model the human decision dynamics. Then, Imitation Learning (IL) based on maximum likelihood estimation is used to train Neural Networks (NN) that map human decisions to observed states. The results show that passive imitation substantially underperforms humans. We further refine the human-inspired policies via Reinforcement Learning (RL), using on-policy algorithms that are more suitable to learn from pre-trained networks. We show that the combination of IL and RL can match human results and that good performance strongly depends on an egocentric representation of the environment. The developed methodology can be used to efficiently learn policies for unmanned vehicles which have to solve missions in an open field environment.

## Author summary

We propose a method to extract control policies from human behavioral data in an open field environment using Imitation Learning (IL). Starting from the imitated policy, we apply Reinforcement Learning (RL) and achieve human-level performance on the same task. We show that RL algorithms combined with IL and an egocentric representation of the environment are the key ingredients for successful learning and for matching human behavior in this type of task. The policies obtained generalize well and rapidly adapt to novel scenarios.

## Introduction

Human beings are exceptional learners: capable of conceiving solutions for individual problems, generalizing acquired skills to new tasks, exploring new strategies, and

inferring causal relationships [1–4]. Since the earliest stage of Machine Learning (ML), the research community has sought to emulate humans’ learning capacities; and only recently, works in the area of reward-based learning, also known as Reinforcement Learning (RL) [5], have accomplished outstanding results in this regard [6]; although, without the same efficiency as humans [7]. A viable option to tackle this issue, again inspired by human learning [8, 9], is to combine reinforcement with imitation in a procedure known as imitation learning (IL) [10, 11]. In this context, it is worth noting that a great number of tasks, such as navigating or exploring unknown environments, are relatively straightforward for humans and can be successfully learned in a limited number of trials. On the other hand, this is often not the case for RL agents, where the amount and the quality of the information retrieved, in addition to the sound design of a reward function and/or a good exploration strategy of the environment, are crucial for successfully learning from scratch. Hence, artificial agents might benefit from imitating human agents.

In this study, we collect movement data from a series of human participants while they are performing a virtual foraging task in which the rewards, in the form of coins, are condensed in clusters throughout the environment. The participants, subject to time constraints, have to collect the highest number of coins, effectively trading-off between foraging within a single cluster (exploitation) and exploration. Humans are initially unaware of the number of clusters and of their locations but are able to learn the reward distribution throughout the course of the experiment. Our main objective is to develop a method based on the combination of IL and RL, which allows artificial agents to efficiently learn the task and eventually match the performance of human agents.

Note that, time-constrained foraging problems occur in several realistic scenarios, including scientific exploration; where, for instance, a rover might want to sample chemical or geological features as fast as possible; or search and rescue operations, where a vessel needs to rescue as many people as possible [12, 13]. Moreover, these missions are dangerous, and the use of aerial or ground unmanned vehicles would significantly mitigate any additional risks. However, without assumptions about the distribution of targets, classical control techniques are not applicable. Tele-operation is also a feasible option, but it may be hindered due to unreliable communications, and this approach does not scale as well as completely autonomous options. For these reasons, ML techniques supporting full autonomy represent an interesting alternative solution to these types of scenarios.

In our experiment, we collected 50 human trajectories and process them to include allocentric and egocentric information in our model. Then, we run IL on each of the trajectories, yielding 50 policies with different performance. None of these policies succeeded in matching human results. We then used the imitated policies as initial solutions and further refined them with RL. By combining the two methods, we outperformed the average human performance and the respective participant from which the agent imitates with a success rate of 78% and 62%, respectively, while using a reasonable amount of training steps ( $\leq 10^7$ ). We also compared our method with a pure RL alternative, and showed that such an approach remarkably underperforms humans.

We also tested the learned policies for generalization and robustness in a new scenario with an unknown reward distribution. We showed that the artificial agents quickly adapt to this new scenario; we conjecture that they rely on an egocentric representation of the environment, as observed in neurophysiological recordings from rodents [14]. To empirically test this hypothesis, we rerun the entire set of experiments only considering allocentric coordinates. We showed that in the absence of an egocentric representation of the environment, RL is unable to further improve IL and the final performance is worse than that of humans.

## Outline and Notation

The remainder of the paper is organized as follows. The Materials and Methods section presents the experimental setup used to collect the human foraging data, introduces the MDP model used for representing human behavior, discusses the IL for learning policies from data, and outlines the RL algorithms used to refine the imitated policies. In the Results section we compare our method with human and RL-only performance on the original setup; then, we test all the artificial agents for robustness to reward distribution shift and demonstrate the importance of egocentric information. We discuss the results in the Discussion section.

**Notation:** Unless otherwise indicated, we use uppercase letters (e.g.,  $S_t$ ) for random variables, lowercase letters (e.g.,  $s_t$ ) for values of random variables, script letters (e.g.,  $\mathcal{S}$ ) for sets, and bold lowercase letters (e.g.,  $\boldsymbol{\theta}$ ) for vectors. Let  $[t_1 : t_2]$  be the set of integers  $t$  such that  $t_1 \leq t \leq t_2$ ; we write  $S_t$  such that  $t_1 \leq t \leq t_2$  as  $S_{t_1:t_2}$ . We denote by  $\mathcal{N}(\mu, \sigma^2)$  the normal distribution, where  $\mu$  is the mean and  $\sigma$  the standard deviation.  $\mathbf{I}$  denotes the identity matrix. We denote the multivariate normal distribution with  $\mathcal{N}(\boldsymbol{\mu}, \sigma^2 \mathbf{I})$  where  $\boldsymbol{\mu}$  is the mean vector and the covariance matrix is diagonal with only  $\sigma^2$  as elements on the diagonal. Finally,  $\mathbb{E}[\cdot]$  represents expectation and  $\mathbb{P}(\cdot)$  probability.

## Materials and methods

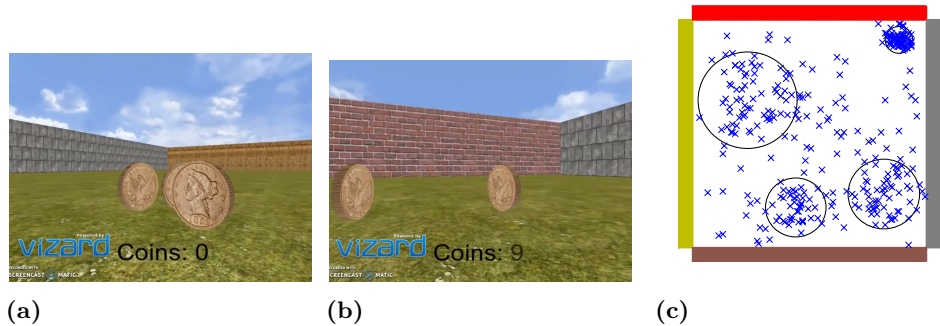


**Fig 1.** Fig. 1a and 1b are two snapshots of the foraging game in which the forager is about to collect coins. Fig. 1c shows a top view of the environment where the coins are indicated by crosses and the coin clusters are indicated by circles.

## Experimental Setup

In the following section, we provide a description of how the human foraging datasets were collected. In S1 Appendix (Fig. 9) and S2 Fig we include an overview of the 50 trajectories used in the IL step. We include datasets, including search trajectories, from five participants taken from a larger study investigating human foraging [15]. An example of two foraging search trajectories is given in Fig. 2.

**Participants:** Participants consisted of male and female, neurologically healthy, English-speaking volunteers between the ages of 18-35 with normal or corrected-to-normal vision. Participants were recruited from Boston University and the surrounding community. Individuals with a history of drug abuse, use of psychoactive medication, neurological or psychiatric disorders, or learning disabilities were excluded.

Additionally, participants with a history of motion sickness when watching or playing video games were also excluded. All participants were compensated and gave written informed consent in accordance with Boston University’s Institutional Review Board.

**Task:** The task consisted of a  $160m \times 160m$  virtual “open-field” paradigm surrounded by four differently colored and textured walls created using Vizard 6.0, a Python-based virtual reality development platform (Fig. 1). 325 coins were distributed throughout the environment, of which 100 were randomly distributed and 225 were distributed according to four different multivariate Gaussian distributions of varying sizes: 75 according to  $\mathcal{N}((60, 75), 5^2\mathbf{I})$ , 40 according to  $\mathcal{N}((-15, -50), 11^2\mathbf{I})$ , 60 according to  $\mathcal{N}((-50, 30), 18^2\mathbf{I})$  and 50 according to  $\mathcal{N}((49, -40), 13^2\mathbf{I})$  (Fig. 1c). Each participant’s starting location was randomized at the beginning of each run. Participants could move forward and turn left or right. They could not move backwards. They were instructed to freely explore the environment and collect as many coins as possible but were not told anything about the distribution or total number of coins. They were also able to see a running count of the coins they had collected for each run. Participants performed the foraging task over two consecutive days. On the first day, naive participants were presented with the task on a desktop computer in a behavioral testing room. On the second day, they performed the same task in an MRI scanner. Subjects performed 10 eight-minute runs on Day 1 and 10 eight-minute runs on Day 2. In the desktop condition (Day 1), participants moved using keyboard arrow keys, and in the scanner (Day 2), they moved using a diamond-shaped button box. For our purposes here, we utilize the 80 minutes of behavioral data from Day 2 of the experiment for 5 participants which collected an average of 243.98 coins each.

## Modeling the Human Decision Process

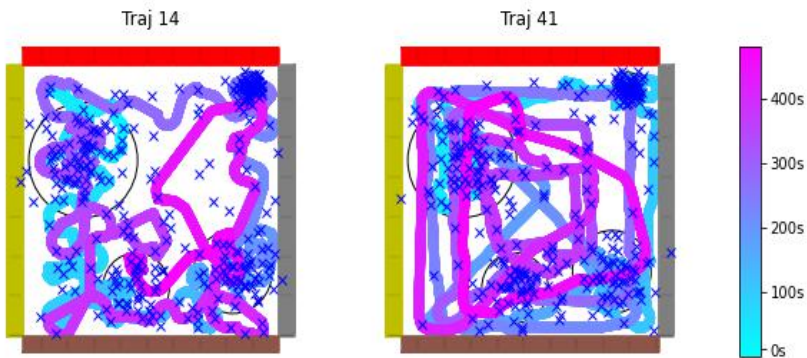


**Fig 2.** Two samples trajectories collected during the second day of tests. The bar on the right shows the time in seconds. The full set of the 50 trajectories is available in S1 Appendix (Fig. 9) and S2 Fig.

In this section we describe how we model the human behavior and how we build the data set and the environment for IL and RL.

We consider an infinite-horizon discounted Markov Decision Process (MDP) defined by the tuple  $(\mathcal{S}, \mathcal{A}, P, r, D, \gamma)$  where  $\mathcal{S}$  is the finite set of states and  $\mathcal{A}$  is the finite set of actions.  $P : \mathcal{S} \times \mathcal{A} \rightarrow \Delta_{\mathcal{S}}$  is the transition probability function and  $\Delta_{\mathcal{S}}$  denotes the space of probability distributions over  $\mathcal{S}$ . The function  $r : \mathcal{S} \times \mathcal{A} \rightarrow \mathbb{R}$  maps rewards to state-action pairs.  $D \in \Delta_{\mathcal{S}}$  is the initial state distribution and  $\gamma \in [0, 1)$  the discount factor. The decision agent is modeled as a stationary policy  $\pi : \mathcal{S} \rightarrow \Delta_{\mathcal{A}}$ , where  $\pi(a|s)$

is the probability of taking action  $a$  in state  $s$ . We parameterize  $\pi$  using a neural network with parameters  $\theta \in \Theta \subset \mathbb{R}^k$  and we write  $\pi_\theta$ .

Given an MDP, we consider the human participants taking into account both egocentric and allocentric strategies when navigating [14, 16]. We define the state vector as  $\mathbf{s} = \{x, y, \psi, \chi\}$ , where  $x, y$  are coordinates with respect to a frame fixed to the environment and represent the allocentric capacities of the agent, i.e., the ability to approximate its current position within the environment. Instead,  $\psi$  and  $\chi$  are two categorical variables that describe the human egocentric behavior: the first tells the agent whether it can see a coin or not in its vicinity,  $\psi \in \{\text{see coin, no coins}\}$ , the second describes the "greedy" direction, i.e., the direction of the closest coin the agent has in its view,  $\chi \in \{\text{east, northeast, north, northwest, west, southwest, south, southeast, no coins}\}$ .

The artificial agent perceives the state and takes an action to interact with the environment. For computational reasons we discretize the  $x, y$  coordinates on a fine grid of  $1m \times 1m$  and define the action space as  $a \in \{\text{east, northeast, north, northwest, west, southwest, south, southeast}\}$ . The transition to the next state always occurs deterministically in the direction of the action  $a$  taken by the agent. As convention in Fig. 2, north means going from bottom to top, south from top to bottom, east is left to right and west vice versa. The categorical state  $\psi$  stays 0 all the time unless there is a coin in a radius of  $8m$  distance, when  $\psi$  turns 1 then also  $\chi$  turns from "no coins" to one of the other directions. This is aligned with the original experiment where each coin pops-up when the human is at  $8m$  from it. Finally, the rewards are simply represented by the coins in the environment where  $r(\mathbf{s}, a) = 1$  for each coin collected. As in the original experiment, the agents automatically collect the reward once at  $3m$  and  $D$  is a uniform distribution over  $\mathcal{S}$ .

## Imitation Learning

Given a task and an agent performing the task, IL infers the underlying agent distribution via a set of an agent's demonstrations (state-action samples). Assuming the agent's behavior is parameterized by a structured parameterization with optimal parameters  $\theta^*$ , we refer to the process of estimating  $\theta^*$  through a finite sequence of agent's demonstrations  $\tau = (\mathbf{s}_{0:T}, a_{0:T})$  with  $2 \leq T < \infty$  as IL. One way to formulate this problem is through maximum likelihood estimation:

$$\max_{\theta} \mathcal{L}(\theta), \tag{1}$$

where  $\mathcal{L}(\theta)$  denotes the log-likelihood and is equivalent to the logarithm of the joint probability of generating the expert demonstrations  $\tau = \{\mathbf{s}_0, a_0, \mathbf{s}_1, a_1, \dots, \mathbf{s}_T, a_T\}$ , i.e.,

$$\mathcal{L}(\theta) = \log \mathbb{P}_D^\theta(\tau). \tag{2}$$

$\mathbb{P}_D^\theta(\tau)$  in (2) is defined as

$$\mathbb{P}_D^\theta(\tau) = D(\mathbf{s}_0) \left[ \prod_{t=0}^T \pi_\theta(a_t | \mathbf{s}_t) \right] \left[ \prod_{t=0}^{T-1} P(\mathbf{s}_{t+1} | \mathbf{s}_t, a_t) \right]. \tag{3}$$

Computing the logarithm of (3) and neglecting the elements not parameterized by  $\theta$  we obtain the following maximization problem

$$\max_{\theta} \sum_{t=0}^T \log(\pi_\theta(a_t | \mathbf{s}_t)). \tag{4}$$

Solving the maximization problem in Eq. (4) is the main objective of our IL step.

## Reinforcement Learning

After defining a model, collecting the data and performing the imitation step, our final goal is to further refine the imitated policies using RL. In RL, the artificial agents are allowed to experience the task themselves and receive a reinforcement according to the reward function  $r(\mathbf{s}_t, a_t)$ . Mathematically, the goal is to find the policy parameters  $\theta$  which maximize the expected total discounted reward  $J(\theta) = \mathbb{E}_\tau[\sum_{t=0}^{\infty} \gamma^t r(\mathbf{s}_t, a_t)]$ , where, as previously,  $\tau = (\mathbf{s}_0, a_0, \mathbf{s}_1, a_1, \dots)$  is sampled according to  $\mathbf{s}_0 \sim D$ ,  $a_t \sim \pi_\theta(\cdot | \mathbf{s}_t)$  and  $\mathbf{s}_{t+1} \sim P(\cdot | \mathbf{s}_t, a_t)$ . Our focus is on model-free RL methods in which the artificial agent does not know the transition probability function  $P(\cdot | \mathbf{s}_t, a_t)$ , and it can only explore the environment and experience rewards. Among these types of algorithms, we can distinguish two main groups: (i) algorithms that update the current policy following the agent’s generated trajectories according to this policy, also known as *on-policy* algorithms, and (ii) algorithms that update the current policy using experience from multiple policies used previously, known as *off-policy*. We provide a more thorough introduction on this difference in the supplementary materials (S1 Appendix).

State-of-art on-policy algorithms include Trust Region Policy Optimization (TRPO) [17], and some robust variants such as Uncertainty Aware TRPO (UATRPO) [18], and Proximal Policy Optimization (PPO) [17]. Whereas, off-policy methods include the Soft-Actor Critic (SAC) [19] and Twin Delayed Deep Deterministic Policy Gradient (TD3) [20]. All these algorithms have proven to achieve outstanding performance in classical RL benchmarks and we will test all of them in our environment.

## Results

In this section, we present our results and describe all the steps that lead to our design. All the code and data to replicate the experiments are accessible at our Github repository.<sup>1</sup> We provide an overview of the NN used to parameterize  $\pi_\theta$  and all the hyperparameters used for each of the IL and RL algorithms in the supplementary materials (S1 Appendix).

### Pre-processing

Our first step is to collect and process the 50 trajectories, of 8 minutes each, recorded on the second day of tests. Each 8-minute trajectory consists of 28973 data points, on average, which means we collect a data point every 0.017s, and the data points are the human agent’s coordinates with respect to the fixed environment frame. Note that it is possible that a human agent does not move for 30s, for example, and then makes many rapid decisions about where to explore in the next few seconds following this stationary period. Therefore, the first 30s could be aggregated in a single data point while the next “few seconds” would require more than a single point. As a result, we aggregate the data points considering the discretization of the  $(x, y)$  coordinates. After that, we go over each of the trajectories and determine the human decisions (i.e., for each aggregated state, the direction of the human’s next movement). We cast each human decision for each trajectory in the pre-determined action space  $\mathcal{A}$  and construct in this way our state-action pairs (i.e., actions  $a$  taken at state  $\mathbf{s}$ ). This process allows us to reduce the average length of human trajectories from 28973 to 3464 data points without losing key information. Note that this processing is an expensive but necessary step for reducing the computational burden and enabling learning. Future research will focus on how to automate this step and developing methods which can handle learning from raw data.

<sup>1</sup><https://github.com/VittorioGiammarino/Learning-from-humans-combining-imitation-and-deep-on-po>

## Imitation Learning

We perform IL on each human trajectory individually rather than considering a single data set with all the trajectories. This is due to two main factors: first, as Fig. 2 shows, each human trajectory covers the majority of the environment; hence, each trajectory is per se informative enough about the task. Second, the trajectories are noisy and a single aggregated data set turns to be too noisy to be beneficial. The results of the IL step and all the details on the evaluation are illustrated, for 5 humans’ trajectories, in Fig 3. In summary, we achieve good learning performance for several trajectories but not enough to match the human participants. A figure showing the IL performance for all the 50 trajectories is available in the supplementary material (S1 Appendix, Fig. 10 and S3 Fig).

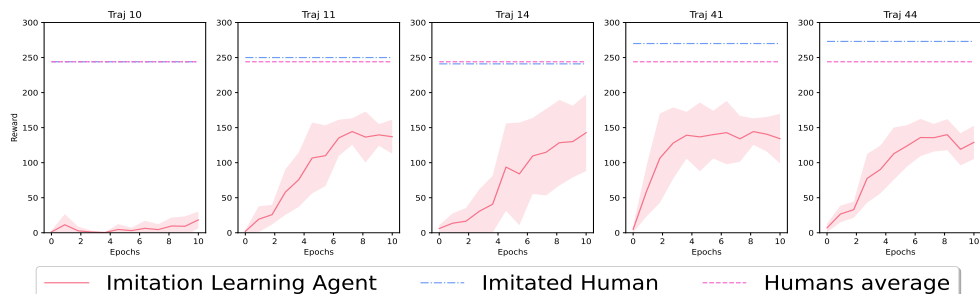


**Fig 3.** The results from the IL step for 5 different human trajectories are illustrated. For each human trajectory we solve the IL problem for 8 different seeds. For each seed, after every epoch we evaluate the performance of the learnt policy for 10 trials, each consisting of 3464 steps. The reported results for the "Imitation Learning Agent" show the reward averaged over 10 trials and 8 seeds; the shaded area shows the standard deviation over the seeds. The performance of the human trajectory used as data set for the imitation is labelled as "Imitated Human". "Humans average" is the average performance of the 50 human trajectories.

## Reinforcement Learning

We consider the 50 policies learnt from the 50 human trajectories during the IL step. We refine these policies using RL. We design the experiment as follows:

1. First, in order to determine which RL algorithm is more suitable for our goal, we take the same single policy learnt during the IL step and use it as initialization of each of the RL algorithms.
2. Given the state-space dimension, we consider  $10^7$  steps as a reasonable amount of steps for performing RL.
3. As in the IL step, for each RL algorithm we run the learning process for 8 random seeds.
4. During the learning process, we evaluate the policy learnt every 30,000 steps on 10 trials of 3464 steps each. We report averaged results over the 10 trials and 8 seeds. The shaded area in Fig. 4 and 5 shows the standard deviation over seeds.
5. After determining the most suitable RL algorithm, we rerun the whole experiment for 50 times in which each of the 50 policies learnt during the IL step is used as initialization of the selected RL algorithm.

Fig. 4 compares the various RL algorithms. PPO outperforms all other methods. Broadly speaking, on-policy algorithms, i.e., PPO, TRPO, and UATRPO, learn more effectively from a pre-initialized policy with respect to the off-policy algorithms TD3 and SAC. Refer to S1 Appendix for more details.

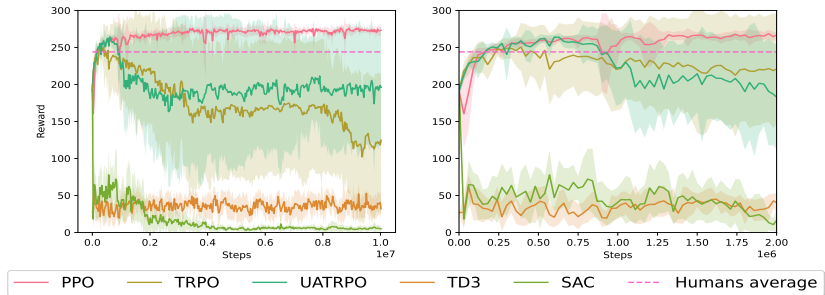


**Fig 4.** The results for the RL algorithms initialized with the same policy are illustrated. For each algorithm we run the learning process for  $10^7$  steps and 8 different random seeds. For each seed, after every 30,000 steps we evaluate the performance of the learnt policy for 10 trials each of 3464 steps. The reported results show the reward averaged over 10 trials and 8 seeds, the shaded area shows the standard deviation over seeds.

Consequently, we proceed by combining IL together with PPO and compare it with the PPO-only alternative. Fig. 5 illustrates the final results for the same trajectories of Fig. 3 and a figure showing this final result for all the 50 trajectories is available in the supplementary material (S1 Appendix, Fig. 11 and S4 Fig). In summary, IL followed by PPO (IL+PPO) outperforms the average human performance and its imitated expert, 39 (78%) and 31 (62%) times, respectively, over the 50 human trajectories. On the other hand, the PPO-only alternative cannot get close to these results in  $10^7$  steps. Table 1 summarizes the comparison between humans and IL+PPO policies with respect to the total amount of collectable rewards.

Note that, Fig. 5 and Fig. 11 provide interesting insights on why pre-training with IL makes sense in foraging tasks with sparse rewards. We observe that, in addition to a different initial performance, the IL+PPO and the PPO-only agents show really different exploration strategies which lead to a different reward convergence rate (the difference in rates is clearly visible both in Fig. 5 and in Fig. 11). The human-inspired exploration strategy of IL+PPO represents the main strength of the method in this setup and the main source of difference with the PPO-only agents. We believe that similar convergence rate can be obtained without directly imitating the human participants provided, however that we can effectively emulate the human exploration strategies. We defer this problem to future work.

## Robustness to reward distribution shift and the importance of egocentric representations

In this section, we test the learnt policies for robustness to a reward distribution shift. The motivation is to explore how quickly the artificial agents grasp changes in the environment and adapt to these changes. As in the original experiment, 325 coins are placed across the environment; however, this time according to the new distribution in Fig. 6a. Specifically, 50 coins are distributed according to  $\mathcal{N}((-70, 30), 5^2\mathbf{I})$ , 75 according to  $\mathcal{N}((60, -20), 11^2\mathbf{I})$ , 100 according to  $\mathcal{N}((-40, 45), 15^2\mathbf{I})$  and 100 according to  $\mathcal{N}((0, 60), 13^2\mathbf{I})$ .

We design the experiment similarly to the RL study and the IL+PPO experiments in Fig. 4 and Fig. 5. Overall, we run, for 8 different random seeds, 100 learning



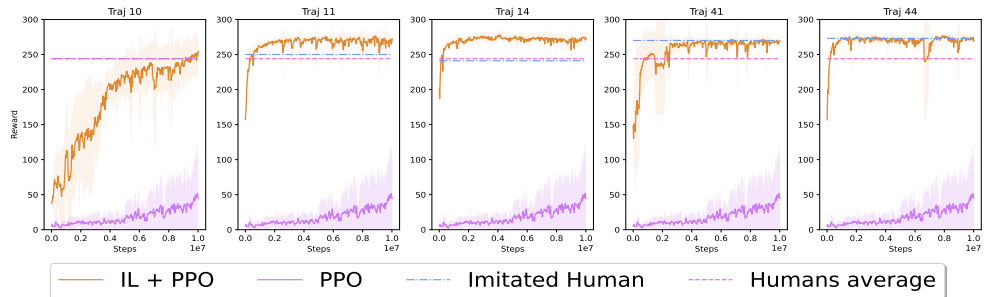


**Fig 5.** The results of the IL+PPO method compared with the PPO-only alternative, the average human performance and the performance of the imitated expert are illustrated for the trajectories of Fig. 3. The experiment design and the reported results follow the same criterion as in Fig. 4.

**Table 1.** A summary of the comparison between IL+PPO and human performance in the original experiment. The table shows the percentage out of 50 learnt policies, for both the IL+PPO and the human agents, where the agent collected at least a certain percentage of rewards. As an example, the table is showing that, for the IL+PPO method, 19 policies (38%) can collect at least 260 coins ( $> 80\%$ ). We compare these results with the human performance where each trajectory is considered as a single human policy. Note that, the IL+PPO policies perform better than humans on average but cannot do better than the best participants.

	Performance Lower Bound			
	$> 70\%$	$> 80\%$	$> 85\%$	$> 90\%$
<b>IL+PPO</b>	88%	38%	0%	0%
<b>Humans</b>	80%	22%	10%	0%

**Table 2.** A summary of the results for the rewards distribution shift experiment. The table shows the fraction out of 50 policies, for each initialization method, where after learning for  $2 \times 10^6$  steps, the agent is able to collect at least a certain percentage of rewards. As an example, the table is showing that, for the IL+PPO initialization, 46 policies (92%) can collect at least 270 coins ( $> 80\%$ ) in this new scenario after learning for only  $2 \times 10^6$  steps.

	Performance Lower Bound			
	$> 70\%$	$> 80\%$	$> 90\%$	$> 95\%$
<b>IL-only initialization</b>	28%	18%	0%	0%
<b>IL+PPO initialization</b>	98%	92%	18%	0%

experiments of  $2 \times 10^6$  steps each, where in the first 50 we initialize using the policies learnt with only IL (Fig. 3), while, in the second 50, we initialize using the policies learnt by IL+PPO (Fig. 5). The results are summarized in Table 2 and show that the policies learnt using both IL+PPO generalize well to novel reward distributions. The figures showing the detailed 100 experiments are available as supplementary materials (S1 Appendix, Fig. 12, 13 and S5 Fig, S6 Fig).

In order to produce these results, we conclude that, given the state vector representation as  $\mathbf{s} = \{x, y, \psi, \chi\}$ , the RL agents and their exploration strategies must heavily rely on egocentric information, i.e., the variables  $\psi$  and  $\chi$ . This would explain the algorithm performance in the novel reward environment in Fig. 6a, where the previously learnt allocentric representation is no longer informative. On the other hand,



(a) New rewards distribution.

(b) Old rewards distribution.

**Fig 6.** Fig. 6a shows the new reward distribution that was not previously seen by any of the artificial agents. We include the previous reward distribution in Fig. 6b to facilitate the comparison.

a strategy based on egocentric exploration which facilitates the generation of a new allocentric representation of the environment would explain the results in Table 2. In other words, we suggest that our IL+PPO algorithms exhibit coding of behavioral variables analogous to the observation in animals (cf. [14]), where electrophysiological recording during foraging strategies indicate neural coding in both egocentric and allocentric coordinate frames.

To demonstrate the veracity of this claim we rerun the entire set of experiments, which includes IL as in Fig. 3 and IL+PPO as in Fig. 5, but this time only providing allocentric information to the artificial agents. In other words, we reduce the state vector from  $\mathbf{s} = \{x, y, \psi, \chi\}$  to  $\mathbf{s} = \{x, y\}$ . The results for a selected number of human trajectories are summarized in Fig 7 and for the entire set of trajectories in S1 Appendix (Fig. 14 and Fig. 15) and S7 Fig, S8 Fig. The final results show that agents trained with the full state  $\mathbf{s} = \{x, y, \psi, \chi\}$  outperform agents trained with the allocentric only state  $\mathbf{s} = \{x, y\}$  74% of the times for IL (37 out of 50) and 100% of the times for IL+PPO. We conclude that our learnt policies heavily rely on egocentric data and that the absence of such information compromises to a large extent the learning performance as illustrated in Fig 7.

## Discussion

In this paper, 50 human navigation trajectories were collected in a virtual open-field environment. We extracted a navigation control policy from each of these trajectories and introduced an MDP setting to capture the navigational human decision making. We learned policies consistent with the experimental data using imitation learning based on log-likelihood maximization for each of the trajectories.

After obtaining a control policy for each trajectory, we used all of them as a starting point for RL, seeking to find policies that can efficiently outperform the human experts in the same experimental setting. We tested state-of-art on-policy (PPO, TRPO, UATRPO) and off-policy (TD3, SAC) algorithms. We explained more extensively how these two categories differ in S1 Appendix in the supplementary material. Briefly, the main element of difference lies in the data used to update the policy network  $\pi_{\theta}$  and in how we compute and approximate the critic network. Off-policy algorithms are usually faster to converge but introduce a large bias in the critic estimate, which results in more oscillatory learning which often jeopardizes the IL initialization. On the other hand, on-policy algorithms are more conservative, where the optimization step is constrained so not to diverge too much from the current policy  $\pi_{\theta}$ . This results in a slower but more steady improvement of performance. Our preference towards PPO with respect to the

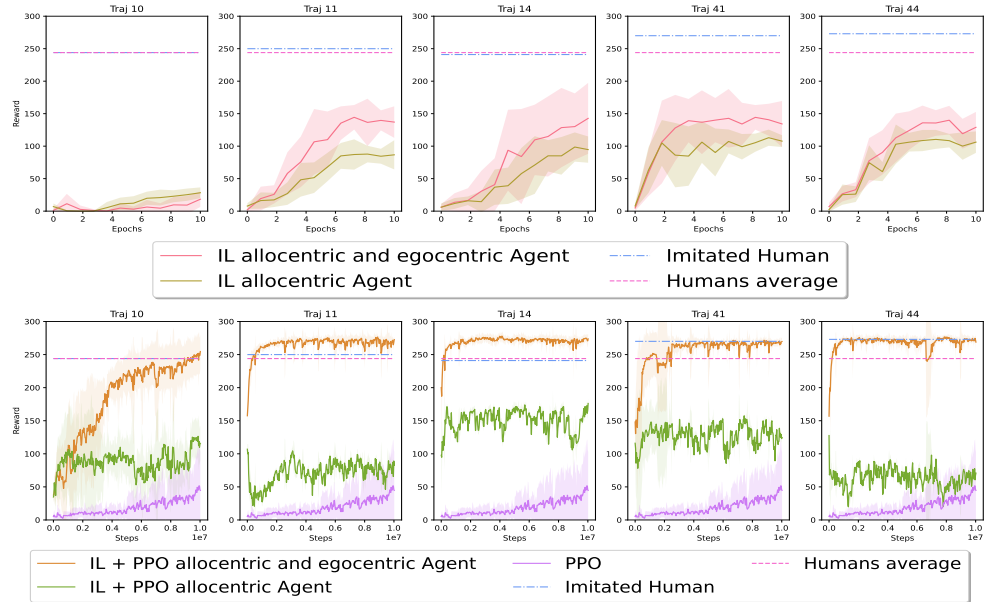


**Fig 7.** Performance comparison for selected trajectories between agent trained with full state including both egocentric and allocentric components  $\mathbf{s} = \{x, y, \psi, \chi\}$  versus an allocentric only state  $\mathbf{s} = \{x, y\}$  for both IL (upper figure) and IL+PPO (lower figure).

other on-policy algorithms is the result of empirical simulation experiments.

Finally, we examined the sensitivity of the IL+PPO and IL-only policies to a different reward distribution and investigated to what extent our artificial agents rely on egocentric information. The final results showed that learning only from data is not enough to match human performance and does not lead to robustness over the reward distribution (Fig. 3, 10 and Table 1). On the other hand, IL followed by PPO (IL+PPO) showed impressive results in the original experiment and it led to good generalization of the task (Fig. 5, 11 and Table 2). Further, we showed that such results are associated with the use of egocentric information, which are crucial in enhancing learning performance both in the IL and the IL+RL setting when compared with the use of allocentric information alone.

In summary, we have developed a method to learn bio-inspired policies from human navigation data, which can be further refined to achieve human-level performance. This approach to modeling human navigational policies can be of great utility for aerial and ground unmanned navigation tasks including scientific exploration and search and rescue operations.

## Supplementary Material

**S1 Appendix.** Text.

**S2 Fig. Humans' Trajectories in the original experiment.** The complete set of 50 8-minutes human trajectories collected during the 2<sup>nd</sup> day of tests.

**S3 Fig. IL complete results.** Results of the IL step for all the 50 human trajectories.

**S4 Fig. IL combined with PPO complete results.** Results of the PPO step with IL initialization for all the 50 human trajectories.

**S5 Fig. New rewards distribution: RL initialized with IL policies.** Results of learning a new rewards distribution with IL-only initialization for all the 50 IL policies in S3 Fig.

**S6 Fig. New rewards distribution: RL initialized with IL+PPO policies.** Results of learning a new reward distribution with IL+PPO initialization for all the 50 policies in S4 Fig.

**S7 Fig. Allocentric only experiment: IL complete results.** Comparison between IL with full state and allocentric-only state for all the 50 human trajectories.

**S8 Fig. Allocentric only experiment: IL combined with PPO complete results.** Comparison between IL+PPO with full state and allocentric-only state for all the 50 human trajectories.

## Acknowledgments

Research was partially supported by the NSF under grants IIS-1914792, DMS-1664644, and CNS-1645681, by the ONR under grants N00014-19-1-2571 and N00014-21-1-2844, by the NIH under grants R01 GM135930 and UL54 TR004130, and by the Boston University Kilachand Fund for Integrated Life Science and Engineering.

## References

1. Walker CM, Williams JJ, Lombrozo T, Gopnik A. Explaining influences children’s reliance on evidence and prior knowledge in causal induction. In: Proceedings of the Annual Meeting of the Cognitive Science Society. vol. 34; 2012.
2. Gopnik A, Griffiths TL, Lucas CG. When younger learners can be better (or at least more open-minded) than older ones. *Current Directions in Psychological Science*. 2015;24(2):87–92.
3. Goddu MK, Lombrozo T, Gopnik A. Transformations and transfer: Preschool children understand abstract relations and reason analogically in a causal task. *Child Development*. 2020;91(6):1898–1915.
4. Ruggeri A, Pelz M, Gopnik A, Schulz E. Toddlers search longer when there is more information to be gained. *PsyArXiv preprint*. 2021;.
5. Shteingart H, Loewenstein Y. Reinforcement learning and human behavior. *Current Opinion in Neurobiology*. 2014;25:93–98.
6. Silver D, Schrittwieser J, Simonyan K, Antonoglou I, Huang A, Guez A, et al. Mastering the game of go without human knowledge. *Nature*. 2017;550(7676):354–359.
7. Botvinick M, Ritter S, Wang JX, Kurth-Nelson Z, Blundell C, Hassabis D. Reinforcement learning, fast and slow. *Trends in Cognitive Sciences*. 2019;23(5):408–422.

8. Offerman T, Sonnemans J. Learning by experience and learning by imitating successful others. *Journal of Economic Behavior & Organization*. 1998;34(4):559–575.
9. Jones SS. The development of imitation in infancy. *Philosophical Transactions of the Royal Society B: Biological Sciences*. 2009;364(1528):2325–2335.
10. Pomerleau DA. Efficient training of artificial neural networks for autonomous navigation. *Neural Computation*. 1991;3(1):88–97.
11. Abbeel P, Coates A, Ng AY. Autonomous helicopter aerobatics through apprenticeship learning. *The International Journal of Robotics Research*. 2010;29(13):1608–1639.
12. Scone S, Phillips I. Trade-off between exploration and reporting victim locations in USAR. In: 2010 IEEE International Symposium on "A World of Wireless, Mobile and Multimedia Networks" (WoWMoM). IEEE; 2010. p. 1–6.
13. Otte M, Correll N, Frazzoli E. Navigation with foraging. In: 2013 IEEE/RSJ International Conference on Intelligent Robots and Systems. IEEE; 2013. p. 3150–3157.
14. Alexander AS, Carstensen LC, Hinman JR, Raudies F, Chapman GW, Hasselmo ME. Egocentric boundary vector tuning of the retrosplenial cortex. *Science Advances*. 2020;6(8):eaaz2322.
15. Moore KN, Yi C, Dunne MF, Stern CE, McGuire JT. Virtual Human Foraging Behavior Follows Predictions for Heavy-Tailed Search. In Society for Neuroscience. 2021;Online.
16. Feigenbaum JD, Morris RG. Allocentric versus egocentric spatial memory after unilateral temporal lobectomy in humans. *Neuropsychology*. 2004;18(3):462.
17. Schulman J, Levine S, Abbeel P, Jordan M, Moritz P. Trust region policy optimization. In: International Conference on Machine Learning. PMLR; 2015. p. 1889–1897.
18. Queeney J, Paschalidis IC, Cassandras CG. Uncertainty-Aware Policy Optimization: A Robust, Adaptive Trust Region Approach. In: Proceedings of the AAAI Conference on Artificial Intelligence. vol. 35; 2021. p. 9377–9385.
19. Haarnoja T, Zhou A, Abbeel P, Levine S. Soft actor-critic: Off-policy maximum entropy deep reinforcement learning with a stochastic actor. In: International Conference on Machine Learning. PMLR; 2018. p. 1861–1870.
20. Fujimoto S, Hoof H, Meger D. Addressing function approximation error in actor-critic methods. In: International Conference on Machine Learning. PMLR; 2018. p. 1587–1596.
21. Sutton RS, Barto AG. Reinforcement learning: An introduction. MIT press; 2018.
22. Sutton RS, McAllester DA, Singh SP, Mansour Y, et al. Policy gradient methods for reinforcement learning with function approximation. In: NIPS. vol. 99. Citeseer; 1999. p. 1057–1063.
23. Queeney J, Paschalidis I, Cassandras C. Generalized Proximal Policy Optimization with Sample Reuse. *Advances in Neural Information Processing Systems*. 2021;34.

24. Kakade S, Langford J. Approximately optimal approximate reinforcement learning. In: In Proc. 19th International Conference on Machine Learning. Citeseer; 2002.

# A Supplementary Material

## A.1 On-policy vs. off-policy RL algorithms

The Dichotomy between on-policy and off-policy reinforcement learning (RL) algorithms started since the earliest days of RL and specifically with temporal-difference (TD) learning. The interested reader can refer to Chapter 6 in [21].

Recall that the goal of RL is to find  $\theta$  such that the expected total discounted reward  $J(\theta) = \mathbb{E}_{\tau}[\sum_{t=0}^{\infty} \gamma^t r(s_t, a_t)]$  is maximized and where  $\tau = (s_0, a_0, s_1, a_1, \dots)$  is sampled according to  $s_0 \sim D$ ,  $a_t \sim \pi_{\theta}(\cdot|s_t)$  and  $s_{t+1} \sim P(\cdot|s_t, a_t)$ . The mechanism used in all the mentioned algorithms consists of alternating policy evaluation with policy improvement and doing it for several iterations until convergence. Specifically, the policy evaluation step consists of using the agent’s policy  $\pi_{\theta}$  to generate trajectories  $\tau = (s_0, a_0, s_1, a_1, \dots)$  to estimate the state-action value function denoted by  $Q_{\theta}(s, a) = \mathbb{E}_{\tau}[\sum_{t=0}^{\infty} \gamma^t r(s_t, a_t) | S_0 = s, A_0 = a]$ , and/or the state value function  $V_{\theta}(s) = \mathbb{E}_{a \sim \pi_{\theta}(\cdot|s_t)}[Q_{\theta}(s, a)]$ . Then, the policy improvement step, updates the current policy  $\pi_{\theta}$  via a policy gradient [22] in a direction that maximizes  $J(\theta)$ .

On-policy algorithms rely only on trajectories  $\tau$  generated by the interaction of  $\pi_{\theta}$  with the environment at the current iteration. Whereas, off-policy algorithms retrieve trajectories generated also at previous iterations and use this past experience in the policy update. This has indeed a different connotation in practice [23]. On-policy methods deliver stable performance throughout learning due to their connection to theoretical policy improvement guarantees (cf. [24]). However, theoretically supported stability yields high sample complexity due to the conspicuous amount of trajectories needed at each iteration. On the other hand, off-policy algorithms address the sample complexity issue by storing data in a replay buffer which are then reused for multiple policy updates. Off-policy methods have proved to be more sample efficient in practice but also more unstable due to the bias introduced in estimating the state-action value function  $Q_{\theta}(s, a)$ . A recent work has sought to combine on-policy algorithms with off-policy ideas [23].

In the specific case of this paper, we observe that the instability due to off-policy updates can undermine the imitation learning (IL) initialization as illustrated in Fig. 8 (see SAC and TD3). At the same time, the IL initialization remarkably helps on-policy methods to accomplish fast and efficient convergence. Thus, IL+PPO results in a more reliable and efficient learning method.

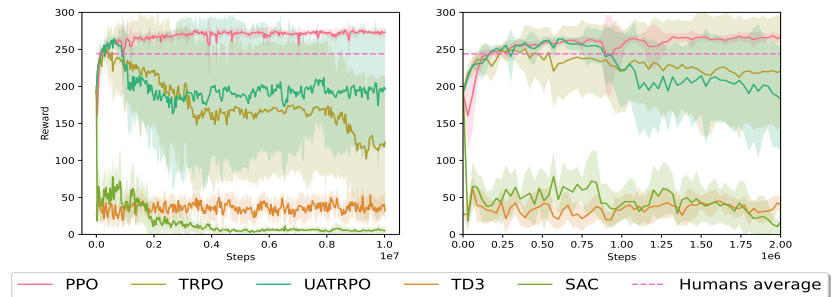


**Fig 8.** The results for the RL algorithms initialized with the same imitation learning policy.

## A.2 Neural Network design

We use the same  $\pi_{\theta}$  architecture for all the algorithms. On-policy algorithms rely on Generalized Advantage Estimation to compute their critic, this method trade-offs

between high variance Monte-Carlo estimation and biased Bootstrap and relies only on the value function network  $V_{\theta_v}$ . On the other hand, off-policy algorithms use TD learning which relies on a state-action value function  $Q_{\theta_q}$ . All the architectures are summarized in Table 3.

**Table 3.** Neural Networks architectures.

$\pi_{\theta}$ network architecture		
Layer type	Dimension	Activation Function
Input	observation size	Linear
Hidden fully connected	128	Relu
Output	action space cardinality	Softmax
$V_{\theta_v}$ network architecture.		
Layer type	Dimension	Activation Function
Input	observation size	Linear
Hidden fully connected	256	Relu
Output	1	Linear
$Q_{\theta_q}$ network architecture.		
Layer type	Dimension	Activation Function
Input	observation size	Linear
Hidden fully connected	256	Relu
Output	action space cardinality	Linear

### A.3 Hyperparameter values, human trajectories and experiments



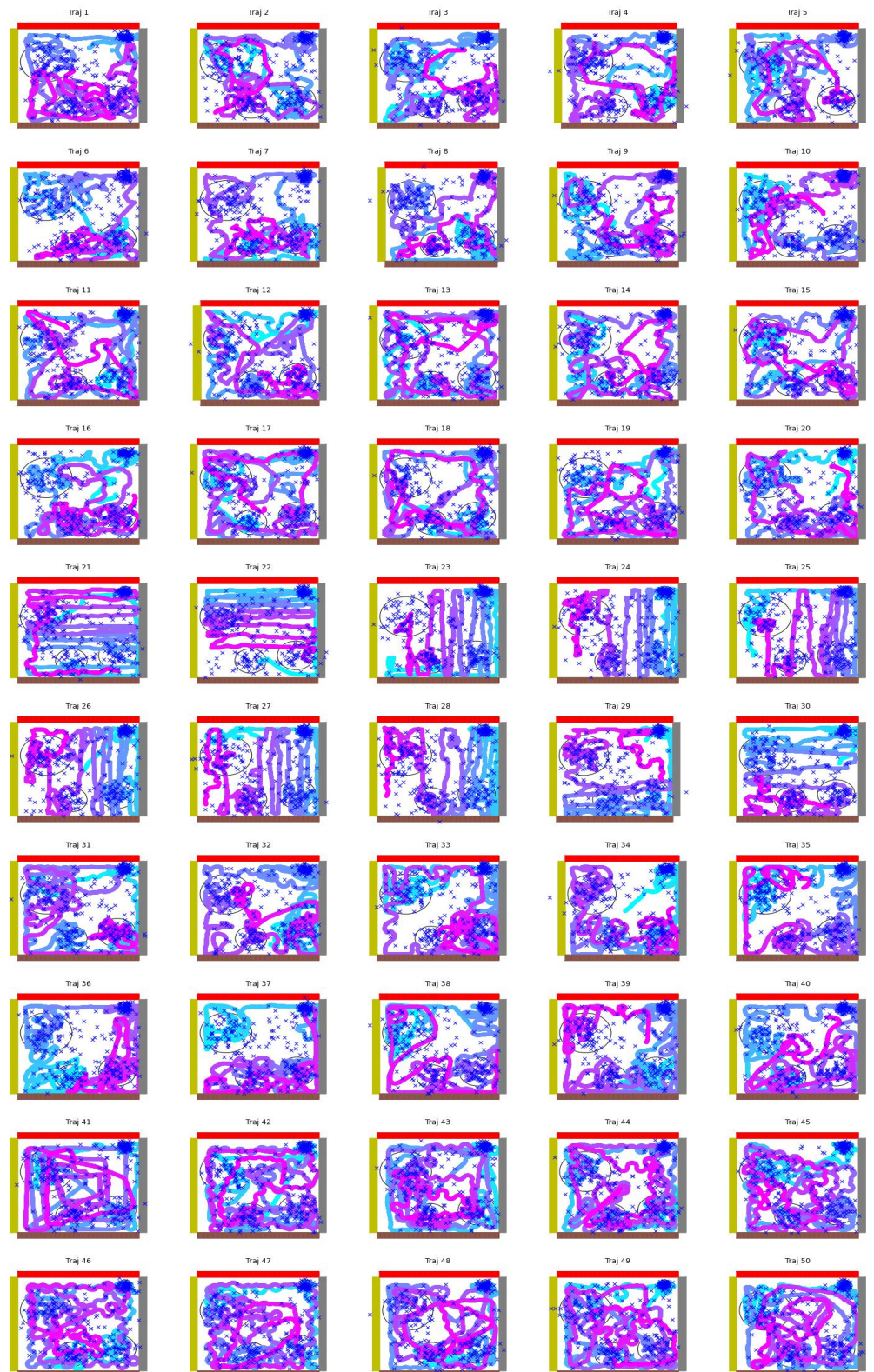


**Fig 9.** The complete set of 50 8-minutes human trajectories collected during the 2<sup>nd</sup> day of tests.

**Table 4.** Hyperparameter values for experimental setup.

Evaluation	Default
Episodes per evaluations	10
Steps per evaluation episode	3464
General IL	
Optimization algorithm	Minibatch gradient ascent
Size minibatches	32
Epochs per update	1
Number of updates	11
Optimizer	Adam
Learning rate	0.001
General RL on-policy	
Max number of steps	$10.02 \times 10^6$
Steps between evaluations	30000
GAE $\gamma$	0.99
GAE $\lambda$	0.99
PPO	
Clipping parameter $\epsilon$	0.2
Entropy	True
Entropy weight $c_2$	$10^{-2}$
Optimization algorithm	Minibatch gradient ascent
Batch size	30000
Size minibatches	64
Epochs per update	10
Optimizer	Adam
Learning rate	$3 \times 10^{-4}$
TRPO	
Trust region parameter $\epsilon$	0.05
Entropy	False
Optimization algorithm	Conjugate gradient ascent with line search
Conjugate gradient damping	0.1
Conjugate iterations per update	20
UATRPO	
Trust region parameter $\epsilon$	0.03
Entropy	False
Optimization algorithm	Conjugate gradient ascent with line search
Conjugate gradient damping	0.1
Conjugate gradient iterations per update	20
Trade-off Parameter ( $c$ )	$6 \times 10^{-4}$
Confidence parameter ( $\alpha$ )	0.05
Number of random projections ( $m$ )	200
EMA weight parameter ( $\beta$ )	0.9

**Table 5.** Hyperparameter values for experimental setup (Cont.).

General RL off-policy	Default
Max number of steps	$10.02 \times 10^6$
Steps between evaluations	30000
Buffer size	$10^6$
Discount $\gamma$	0.99
Optimization algorithm	Batch gradient ascent
Batch size	256
Optimizer	Adam
Learning rate	$3 \times 10^{-4}$
SAC	
Entropy temperature init $\alpha$	0.2
Target critic update step ( $\tau$ )	0.005
TD3	
Exploration noise std	0.1
Policy Noise std	0.2
Noise clip	0.5
Update steps delay	2
Target critic and policy update step ( $\tau$ )	0.005

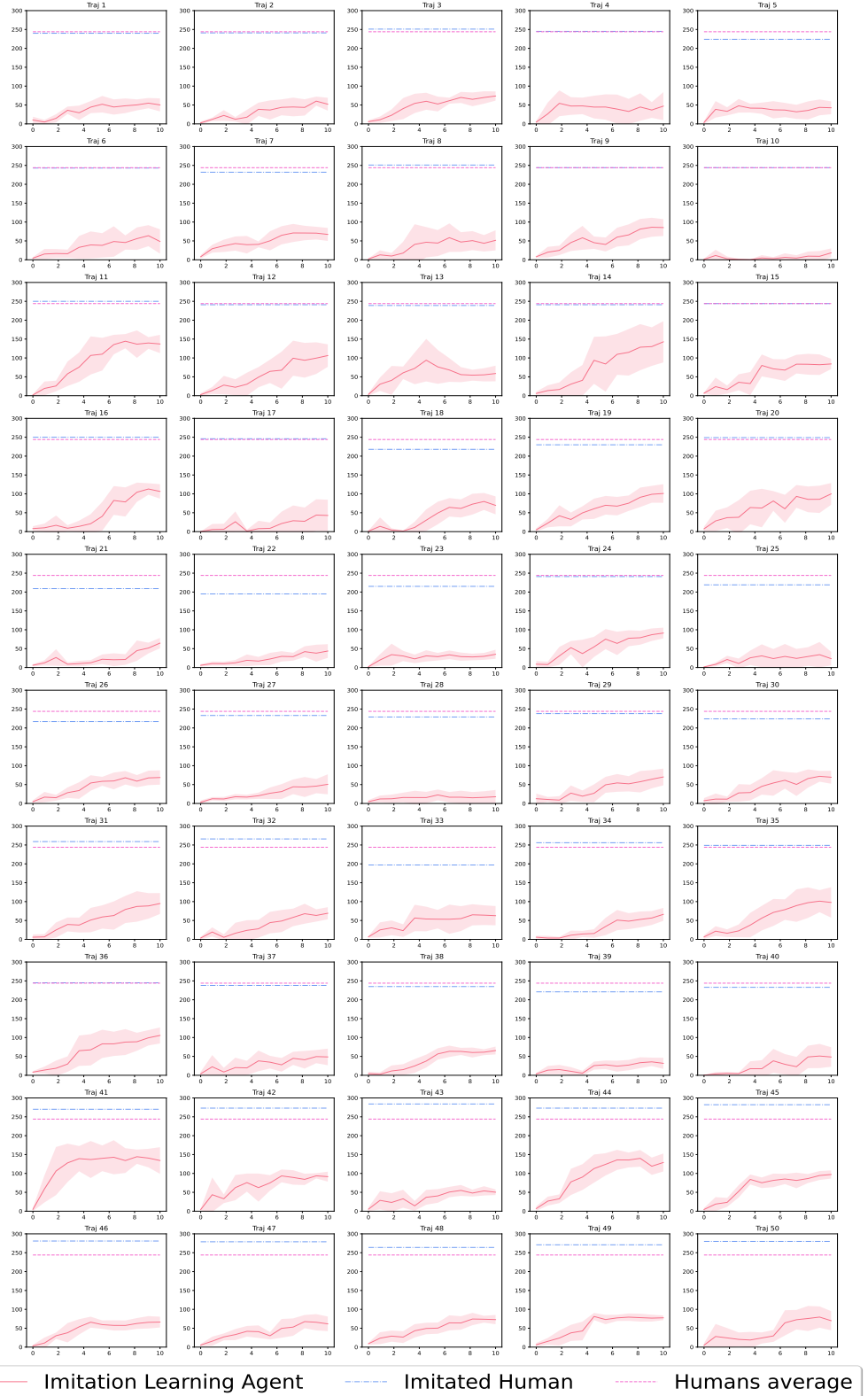


**Fig 10.** Results of the IL step for all the 50 human trajectories in Fig. 9.

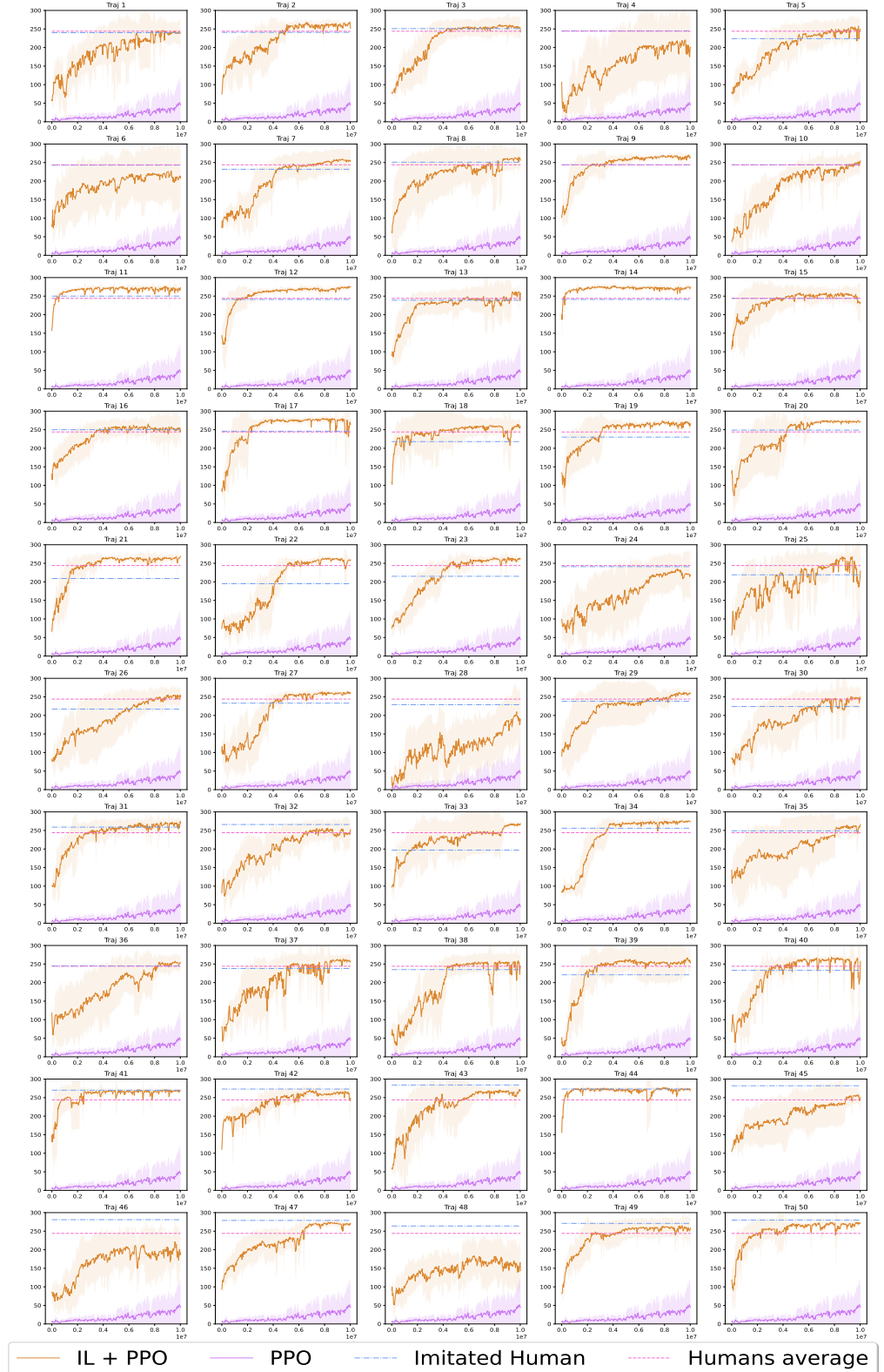


**Fig 11.** Results of the PPO step with the 50 IL policies in Fig. 10.

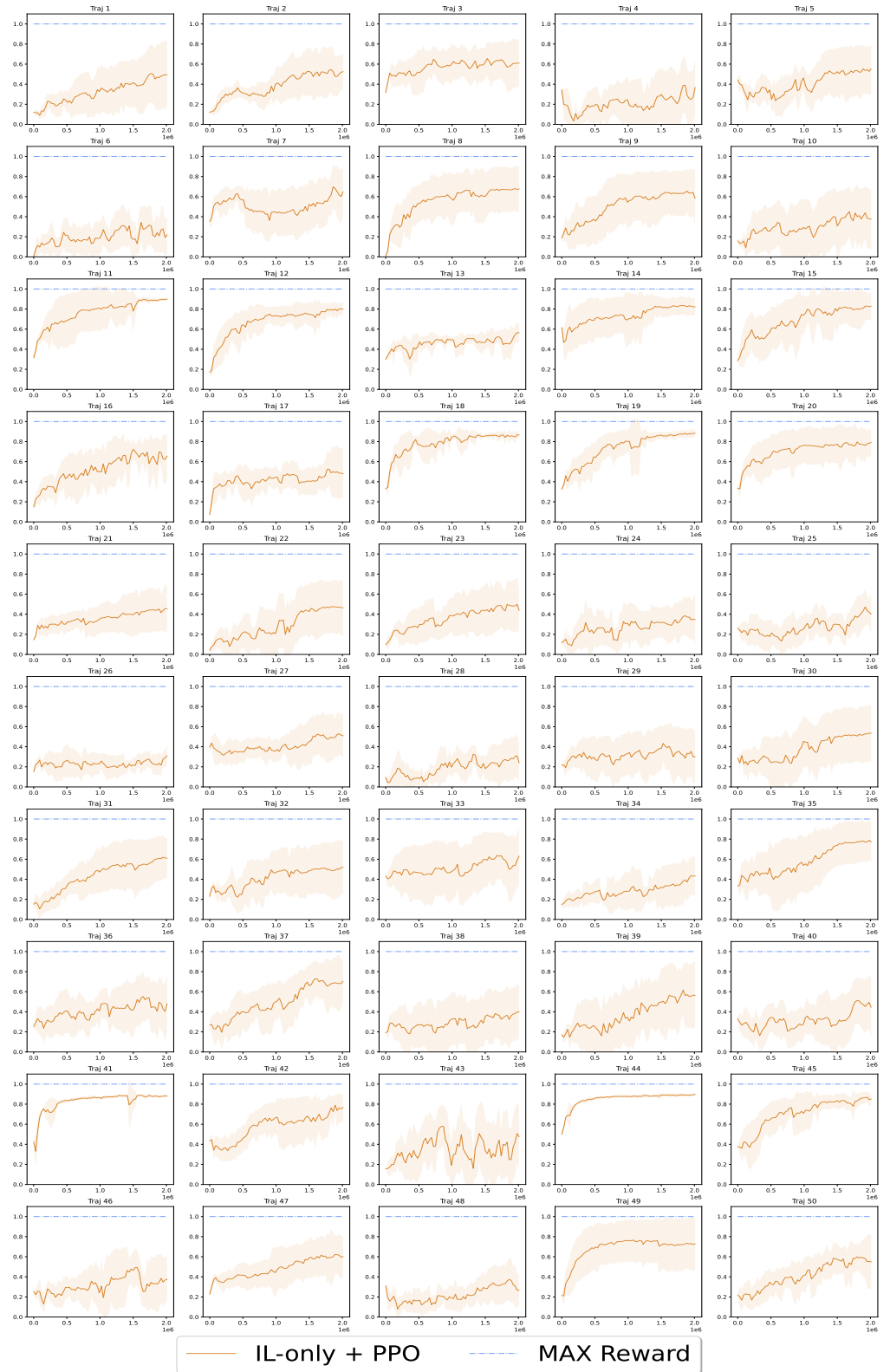


**Fig 12.** Results of learning a new rewards distribution in Fig 6a with the IL-only initialization for all the 50 IL policies in Fig. 10.



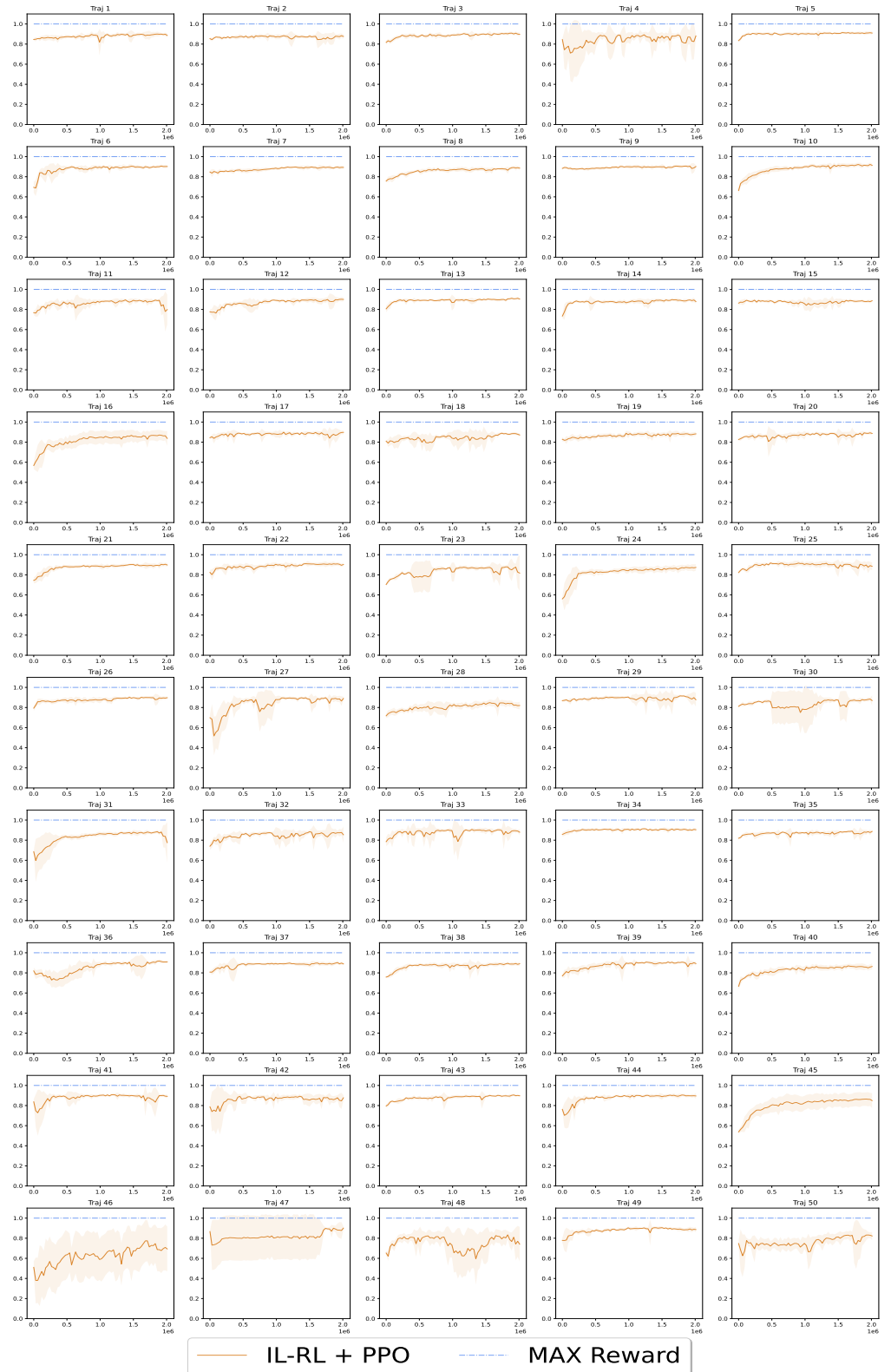


**Fig 13.** Results of learning a new rewards distribution in Fig 6a with IL+PPO initialization for all the 50 policies in Fig. 11.

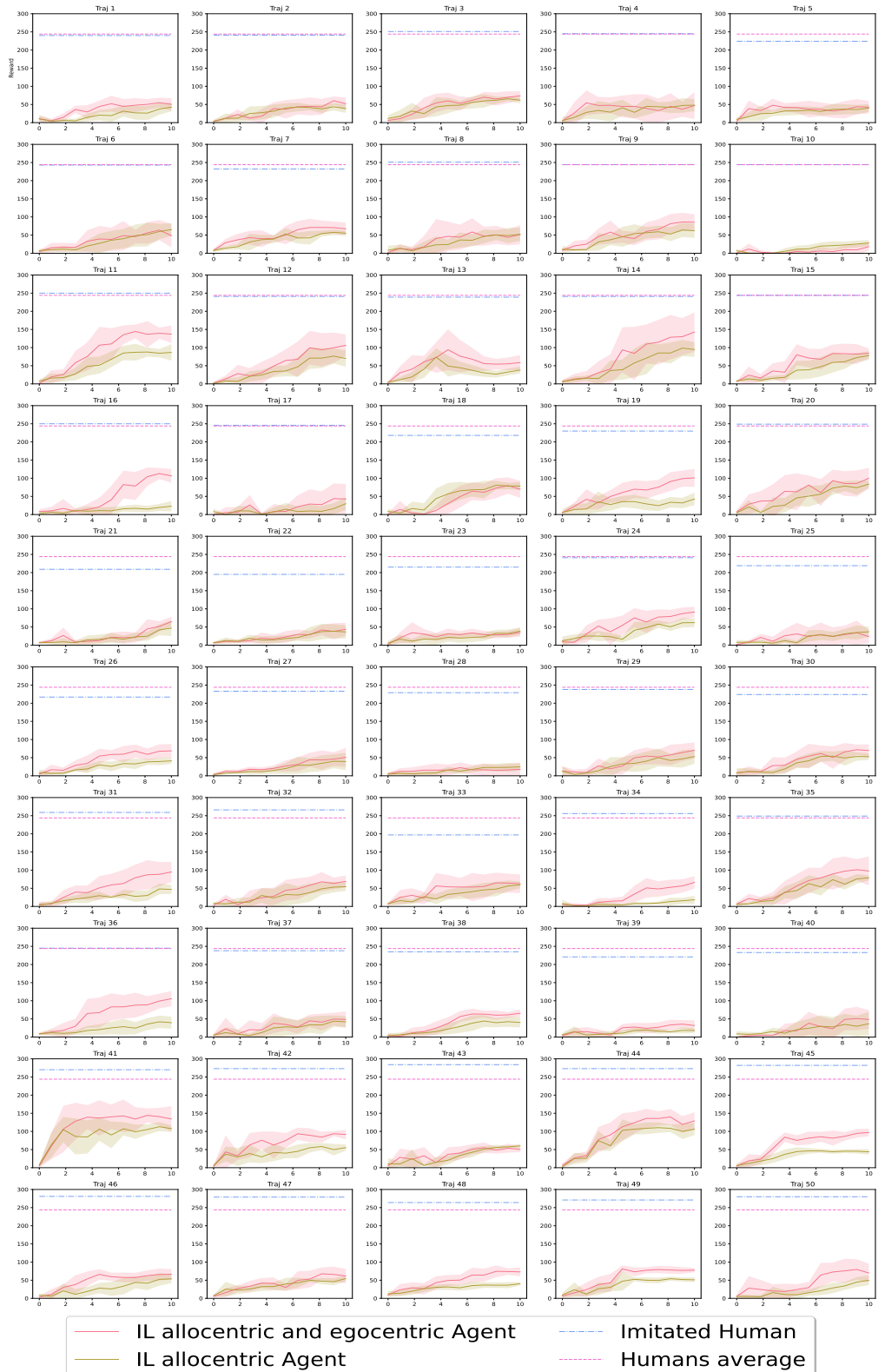


**Fig 14.** Comparison between IL with full state and allocentric only state for all the 50 human trajectories.



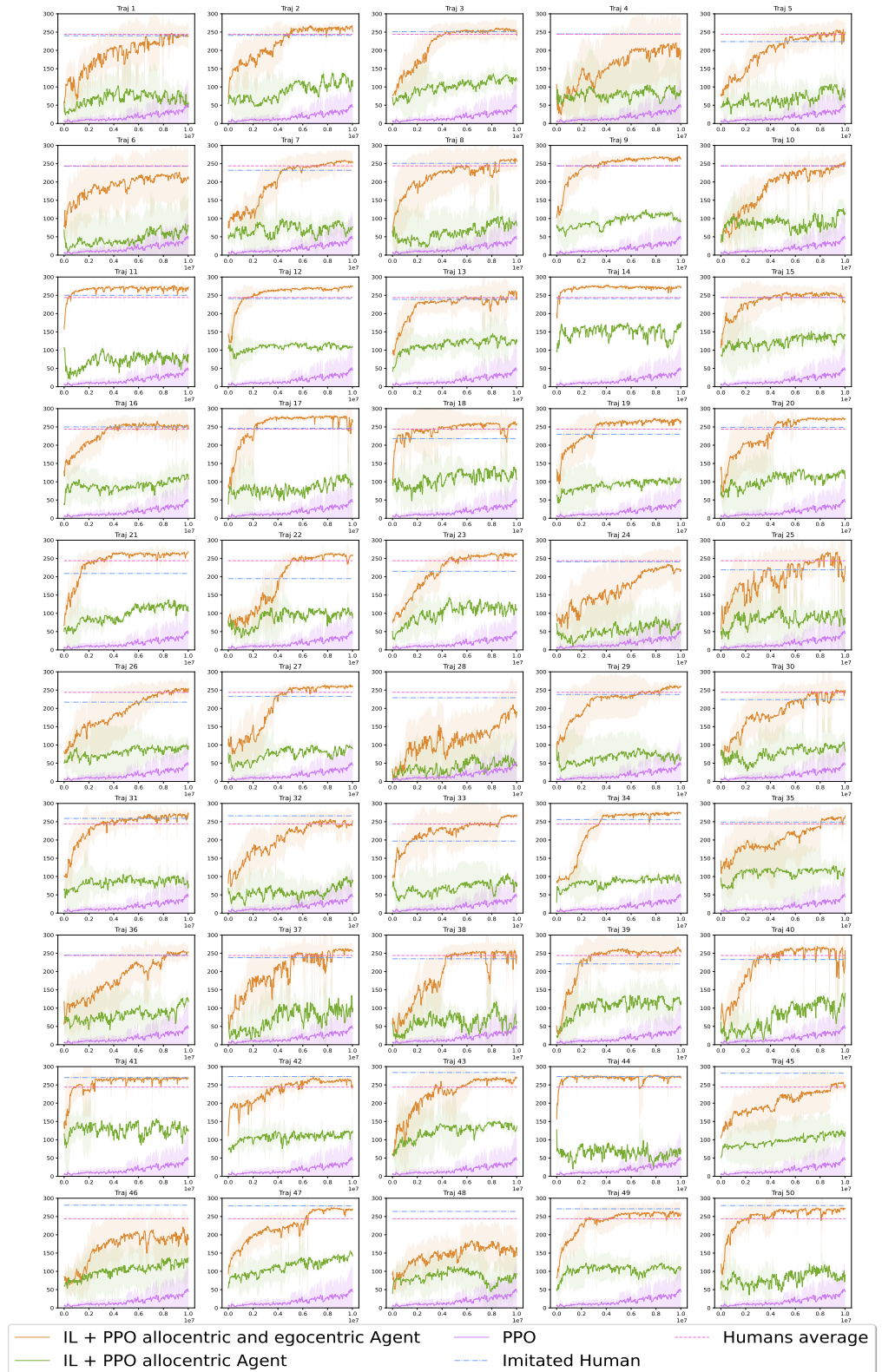


**Fig 15.** Comparison between IL+PPO with full state and allocentric only state for all the 50 human trajectories.